Post-print of an article accepted in *International Journal of Damage Mechanics.* The final, definitive version of this paper has been published as DOI: http://dx.doi.org/10.1177/1056789515569088 .

Effects of heat treatment and strain rate on the microstructure and mechanical properties of 6061 Al alloy

Ling Li, E.A. Flores-Johnson*, Luming Shen, Gwénaëlle Proust
School of Civil Engineering, The University of Sydney, Sydney, NSW 2006, Australia

Abstract: In the present work, the effects of heat treatment and strain rate on mechanical behaviour and microstructure evolution of aluminium alloy (AA) 6061 have been investigated. The micro-crack initiation and crystallographic texture evolution are obtained from scanning electron microscope (SEM) and electron back-scatter diffraction (EBSD) experiments. Quasi-static and high strain rate compression tests are conducted on AA6061 specimens that underwent two different heat treatments: the as-received material with the original T6 heat treatment and the heat treated and artificially aged (HT) specimens. For the high strain rate compression (~2000 s^{-1} and ~4000 s^{-1}) tests, the split Hopkinson pressure bar apparatus is used. It is observed that the additional heat treatment has significantly reduced the yield strength of the material. Furthermore, EBSD results show that the higher the applied strain rate is, the less significant change will happen to the texture. SEM images show that, for both T6 and HT specimens, the number and size of micro-cracks in the dynamic compressed specimens are smaller than in the quasi-static deformed specimen. Therefore, the strain rate is considered to be the dominant factor in forming micro-cracks.

Keywords: Aluminium alloy 6061, high strain rate testing, split Hopkinson pressure bar, microstructure, EBSD.

*Corresponding author: Tel.: +61 2 9351 2113; fax: +61 2 9351 3343.
E-mail address: emmanuel.flores-johnson@sydney.edu.au

Introduction

Solution heat treatment and artificial aging are common processes in metallurgy to improve the mechanical performance of metals (Sadeler et al. 2004; Senkov et al. 2008; Han et al. 2011). The process parameters employed during these treatments are shown to play an important role in the mechanical properties of alloys (Adrien et al. 2004; Harnish et al. 2005; Liu et al. 2010; Ma et al. 2010). Strain rate is another significant factor that influences mechanical behaviour (Oosterkamp et al. 2000; Flores-Johnson et al. 2012; Johnsen et al. 2013). When the materials are used in circumstances that involve high strain rate deformation, such as in the automotive, aerospace and defence industries, it is essential to consider the effect of high strain rate deformation (Lee et al. 2000). For instance, a typical application of aluminium alloy (AA) 6061 is manufacturing automotive parts such as the automobile body panels and wheel spacers (Ozturk et al. 2010). In case a car crash accident happens, these components will be subjected to high strain rate deformation which may lead to failure of the materials. In fact, the mechanical behaviour of the component depends not only on the strain rate but also on its microstructure evolution (Lee et al. 2000). A large number of studies have been devoted to the dynamic mechanical and thermal behaviours of

aluminium alloys (for example see (Wagenhofer et al. 1999; Moustafa et al. 2003; Sadeler et al. 2004; Smerd et al. 2005)) and they have shown that heat treatments and rate of deformation have a great influence on the mechanical response of these alloys .

The effect of heat treatment on microstructure and mechanical properties has been studied on various aluminium alloys (Mrowka-Nowotnik and Sieniawski 2005; Senkov et al. 2008; Marlaud et al. 2010; Maisonnette et al. 2011). Specifically, Poole et al. (2000) studied the effect of solution heat treatment and subsequent artificial aging on the mechanical properties of AA7030 and AA7108 alloys. They attributed the reason of the decrease of the magnitude of the peak strength to the widening of the precipitate size distribution. Some other work focused on the effect of strain rate on mechanical behaviour of aluminium alloys (Xu et al. 2001; Han et al. 2006). Lee et al. (2000) investigated the effect of strain rate on the microstructure evolution, the fracture mechanisms and the occurrence of shear localization on AA7075 using a split Hopkinson bar. They observed that the compression response of the material is sensitive to the applied strain rate and test temperature, and the adiabatic shearing is responsible for the crack formation. A similar conclusion of the function of adiabatic shear bands to the crack formation was drawn by Odeshi et al. (2007) through dynamic loading experiments on AA6061-T6 composite. Garrett et al. (2005) experimentally showed the effects of solution heat treatment time on the mechanical properties at a range of deformation rates through a series of thermal-mechanical tests on AA6082. They introduced a solution heat treatment completeness variable to describe the microstructural evolution of the material during the heat treatment process. Nonetheless, the strain rates they used were not higher than 10 s^{-1}. Lassance et al. (2007) concluded from observations of fracture in 6XXX Al alloys at room and high temperatures that the damage evolution depends on the strain rate sensitivity of the matrix surrounding the voids.

Despite the importance of the effects of heat treatment and strain rate on aluminium alloys, the relationship between these effects and the damage of material has not yet been fully explored and discussed, nor the microstructure and crystallographic texture evolution during dynamic impact deformation. Therefore, for this paper, a heat treatment on a commercial AA6061 alloy has been carried out, and comparison between the mechanical response and texture evolution under different strain rates for the as-received and heat treated (HT) specimens were performed. The split Hopkinson pressure bar (SHPB) test is adopted to apply high strain rate compression on the specimens, and scanning electron microscope (SEM) and electron back-scatter diffraction (EBSD) characterisations are performed to obtain the crack initiation and texture evolution after compression. The effects of heat treatment and strain rate on the microstructure evolution and mechanical properties are then studied.

The remaining sections of the paper are organised as follows. The experimental procedure of heat treatment, mechanical testing and characterisation of microstructure and texture of the specimens are explained in section 2. The results of quasi-static and high strain rate compressions, microstructure and crystallographic texture evolution are presented in section 3. Section 4 discusses the effects of heat treatment and strain rate on the mechanical behaviour and damage of the material. The conclusions are given in the last section.

Experimental Procedure

Material

Cylindrical specimens with heights of 3.9 and 7.8 mm for both quasi-static and high strain rate testing were cut from commercially available AA6061 tempered grade T6. The material was supplied in the form of extruded rods, 6.35 mm in diameter. A second batch of cut samples were solution heat treated and artificially aged as described in the next section. The chemical composition of AA6061-T6 is listed in Table 1 (Tucker et al. 2010).

Table 1. Chemical compositions of AA6061-T6 (Tucker et al. 2010)

Composition	Al	Cr	Cu	Fe	Mg	Mn	Si
Content (%)	95.8-98.6	0.04-0.35	0.15-0.40	<0.7	0.8-1.2	<0.15	0.4-0.8

Heat treatment

The specimens were first solution heat treated at 550 ºC in a salt bath to homogenise the microstructure. Then the specimens were placed in an oil bath for 30 minutes at 200 ºC to modify the microstructure and see the effect of heat treatment on the mechanical response of the material. The ageing time and temperature were chosen according to Ozturk et al. (2010).

Mechanical testing

The specimens, with and without additional heat treatment, were tested under uniaxial compression at quasi-static and high strain rate loadings. The quasi-static uniaxial compression tests were conducted in a 50 kN servo-hydraulic universal testing machine MTS-43 at a strain rate of 5×10^{-4} s^{-1} up to 20% true strain using specimens of 7.8 mm in length.

The high-strain rate tests were performed using a 15 mm diameter SHPB at room temperature. The 15 mm diameter bars were made of high strength steel with yield strength of 1.3 GPa. To achieve strain rates of ~2000 s^{-1} and ~4000 s^{-1}, specimens with lengths of 3.9 mm and 7.8 mm were used, respectively. A ~20% true strain was achieved in the specimens by employing high strength steel stopper rings with an inner diameter of 9 mm and an outer diameter of 15 mm during the dynamic testing. Results obtained without stopper ring (larger strains), which are not presented here, demonstrated the repeatability of the tests.

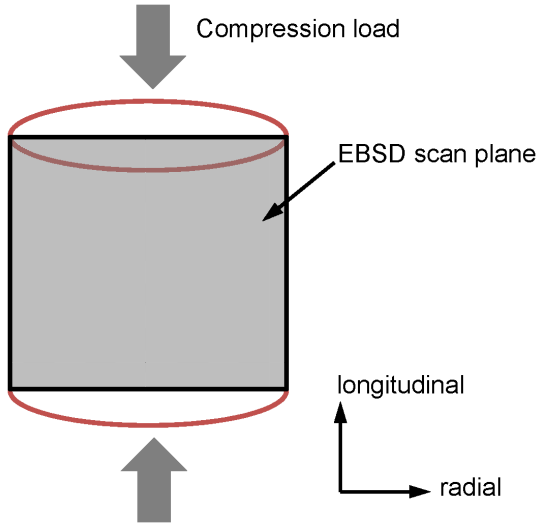

Fig.1. Schematic of the plane scanned in EBSD experiments.

Characterisation of microstructure and texture

The microstructure and crystallographic texture of AA6061 were acquired through EBSD experiments that were conducted using a Zeiss ULTRA plus SEM equipped with Oxford Instruments AZtec integrated energy-dispersive spectroscopy (EDS) and EBSD system. All specimens were examined at an accelerating voltage of 20 kV and the scan step size was chosen to be 0.5 µm. The specimens were cut in the transverse direction and the longitudinal-transverse plane of the specimen, as shown in Fig.1. The undeformed texture of T6 specimen was obtained from respective EBSD scans of two samples and their crystallographic textures were the same. For the undeformed HT specimen and other deformed specimens, one sample for each loading condition was scanned. The loading direction is in the vertical direction of the scanned surfaces. The

microstructures are presented by EBSD inverse pole figure maps and the textures by recalculated pole figures with the HKL Channel 5 system. Furthermore, the histograms of grain size, boundaries and local misorientation distributions are calculated from the EBSD results and compared in the next section.

Results

Mechanical response

Typical true stress-true strain curves from quasi-static and SHPB compression tests are given in Fig. 2. Test results at three strain rates for as-received (6061-T6) and in-house heat treated (6061-HT) specimens are compared. As shown in Fig. 2, the yield strength σ_y of 6061-T6 under quasi-static compression (5×10^{-4} s^{-1}) is 335 MPa. For high strain rates of 2000 s^{-1} and 4000 s^{-1}, σ_y is 370 MPa and 391 MPa, respectively, indicating increases of 10% and 17% when compared to the quasi-static yield strength. This mechanical behaviour is similar to that reported for 6061-T6 in (Tucker et al. 2010) and shows the well-known strain rate dependence of this Al alloy (Hoge 1966). At 20% true strain, the increases of strength, when compared to the quasi-static compression strength (402 MPa), are 8% and 14% for 2000 s^{-1} and 4000 s^{-1}, respectively.

Also it can be seen from Fig. 2 that, the heat-treated 6061-HT specimens show a substantial reduction of the yield strength when compared to the 6061-T6 specimens. For the heat treated specimens, σ_y is 168 MPa under quasi-static compression. At high-strain rates of 2000 s^{-1} and 4000 s^{-1}, σ_y is 187 MPa and 199 MPa, respectively, indicating increases of 15% and 19% when compared to the quasi-static yield strength of the heat-treated specimen. Moreover, although the additional heat treatment has resulted in slightly larger strain rate sensitivity on the yield strength, the 8.9% increase of strength at 20% true strain for HT specimens is smaller than that of 14% increase for T6 specimens, showing that the heat treatment has reduced the strain rate sensitivity at large strains.

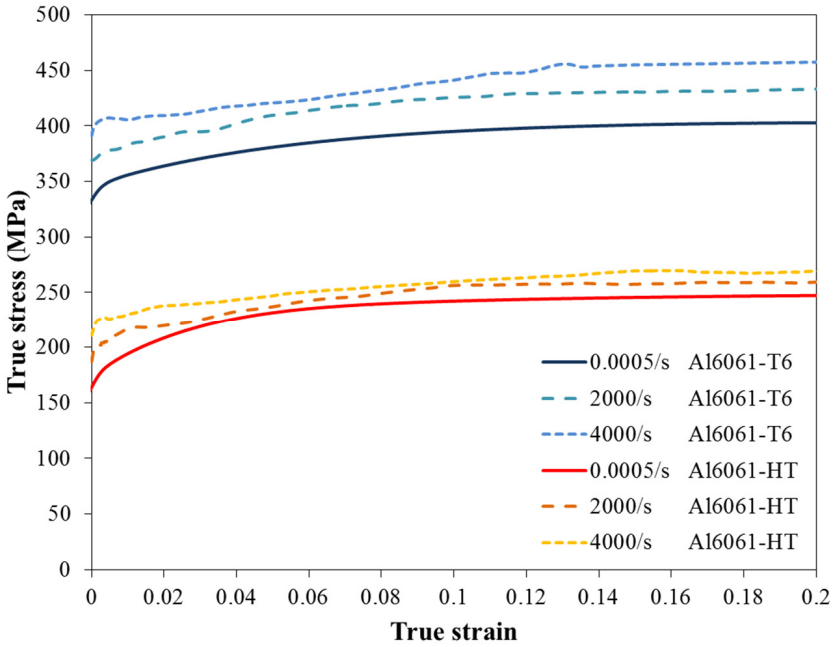

Fig.2. Typical stress-strain curves of AA6061-T6 and AA6061-HT under uniaxial compression at different strain rates.

Microstructural evolution

The initial local misorientation distribution maps of T6 and HT specimens obtained from EBSD

are compared in Fig. 3. It is clear from Fig. 3(b) that the additional heat treatment has reduced the local misorientation density and only a couple of grains contain intragranular misorientations. The T6 specimen was extruded and a host of residual internal strains were found in the specimen. The heat treatment that HT specimens underwent not only changed the distribution and size of the precipitates but also annealed a large number of dislocations. After 20% strain compression, the local misorientation densities have been dramatically increased for both T6 and HT specimens at all strain rates, as shown in Fig. 4. It can be seen from Fig. 4 that the compression has induced a large number of dislocations within grains and some of them have even evolved into grain boundaries. As a result, the compression significantly increased the frequency of low angle grain boundaries. This observation is also confirmed from Fig. 5 which shows the comparison of statistical distributions of microstructural properties in the specimens deformed by 20% strain under different strain rates. It is clear in Fig. 5(a) and 5(b) that the compression has produced a widely spread distribution of misorientation angles, which means the number of subgrain boundaries within each grain has been dramatically increased after deformation. It is also shown in Figs. 5(a) and (b) that the distributions of misorientation angles are very similar for all strain rates for both T6 and HT specimens.

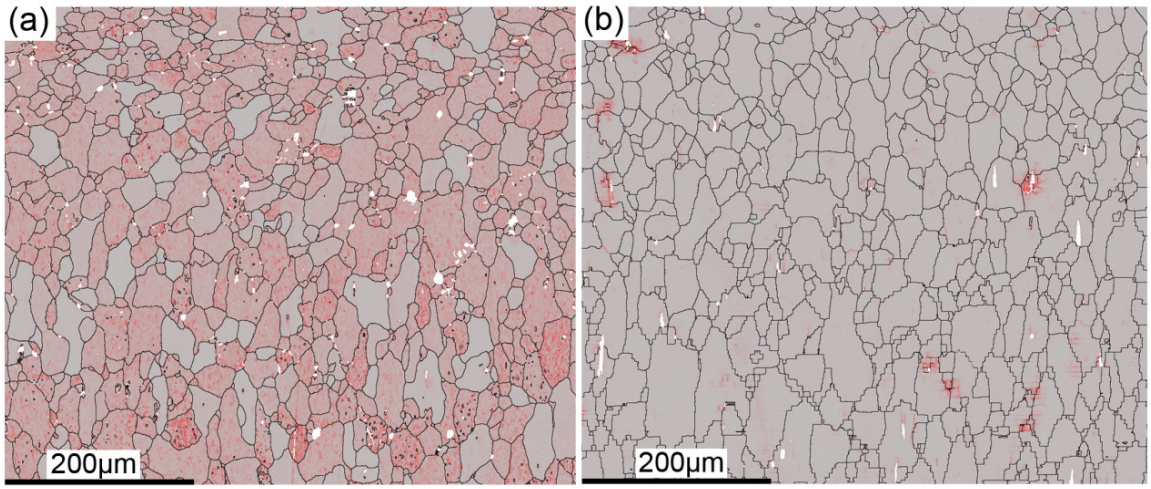

Fig. 3. Local misorientation distribution maps of undeformed (a) T6 and (b) HT specimens from EBSD tests. Black lines are grain boundaries.

The statistics of grain size and grain boundary distributions with respect to different strain rates for both T6 and HT specimens are given in Fig. 5(c)-(f), respectively. As can be seen from Fig. 5(c) and 5(d), the quasi-static and 4000 s^{-1} strain rate compressions resulted in similar grain size distributions on both T6 and HT specimens. Fig. 5(e) and 5(f) indicate that the grain boundary distributions of the HT specimens have remarkably changed after compression. Nonetheless, the difference between different strain rates is only slightly larger than the T6 specimens.

Furthermore, the effect of additional heat treatment can be understood by comparing grain size, boundary and local misorientation distributions between T6 and HT specimens in Figs. 6-8, respectively. As shown in Fig. 6(a), the additional heat treatment has reduced the number of small grains and produced more grains with diameter of 10-30 μm in the HT specimens through the annealing of dislocations and a slight grain growth process. However, after the compression test, the grain size distributions of T6 and HT specimens are almost the same, regardless of strain rates. In terms of grain boundary distributions, Fig. 7 shows that the compressions at strain rate of 5×10^{-4} s^{-1} (Fig. 7(b)) and 2000 s^{-1} (Fig. 7(c)) produced similar grain boundary distributions even though the initial distributions are very different in T6 and HT specimens, while the 4000 s^{-1} strain rate (Fig. 7(d)) resulted in a larger gap between T6 and HT specimens. Moreover, the initial T6 specimens

contain larger misorientation angles than in the HT specimens as shown in Fig. 8(a). However, after compression, the deformed distributions at strain rates of 2000 s^{-1} and 4000 s^{-1} (Fig. 8(c) and 8(d)) are almost identical, while the quasi-statically compressed HT specimens have slightly higher distribution than their counterparts, as shown in Fig. 8(b).

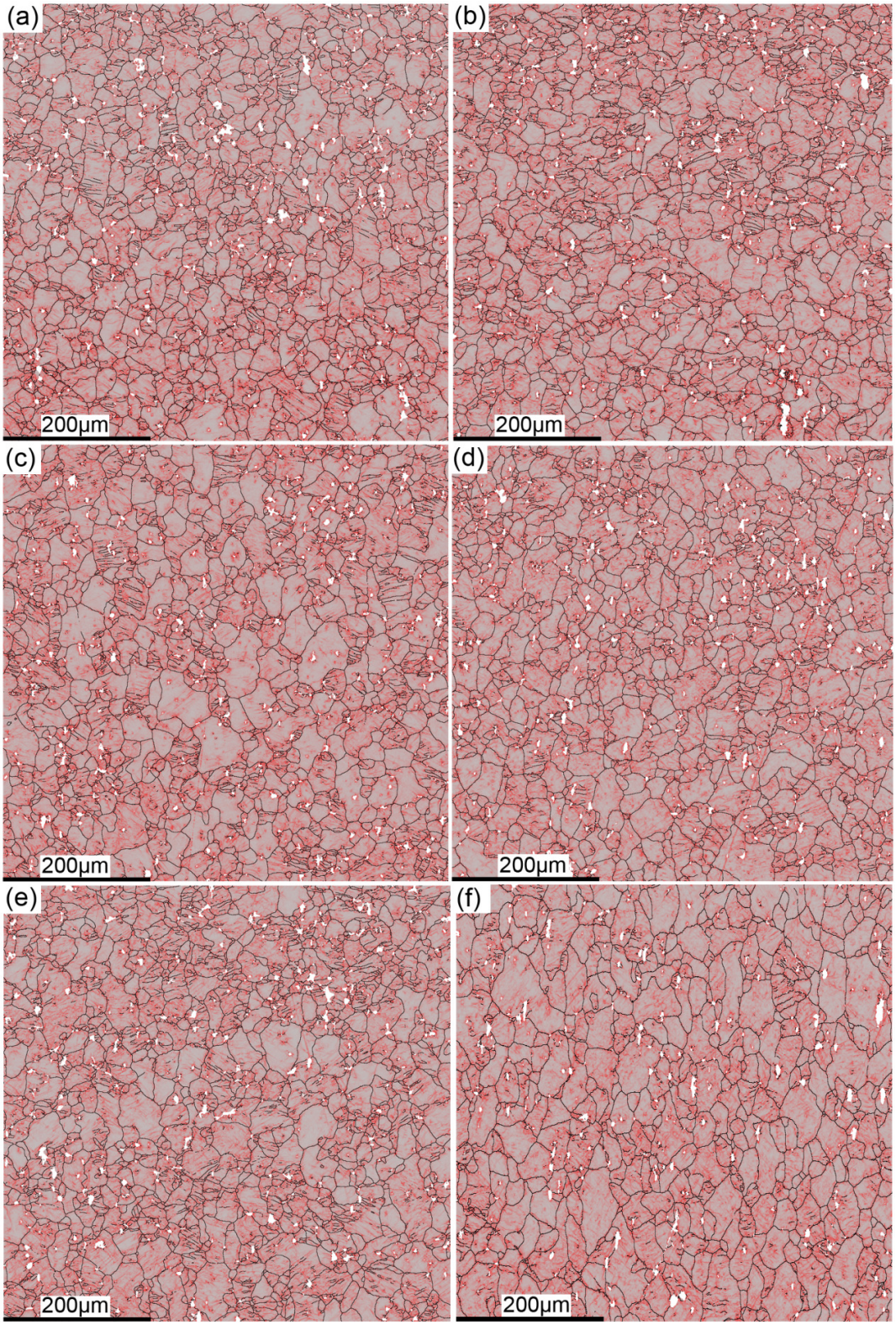

Fig. 4. Local misorientation distribution maps of T6 (left column) and HT (right column) specimens. (a) and (b) are after quasi-static (5×10^{-4} s^{-1}) compression, (c) and (d) are after 2000 s^{-1} dynamic compression, and (e) and (f) are after 4000 s^{-1} dynamic compression. Black lines are grain boundaries.

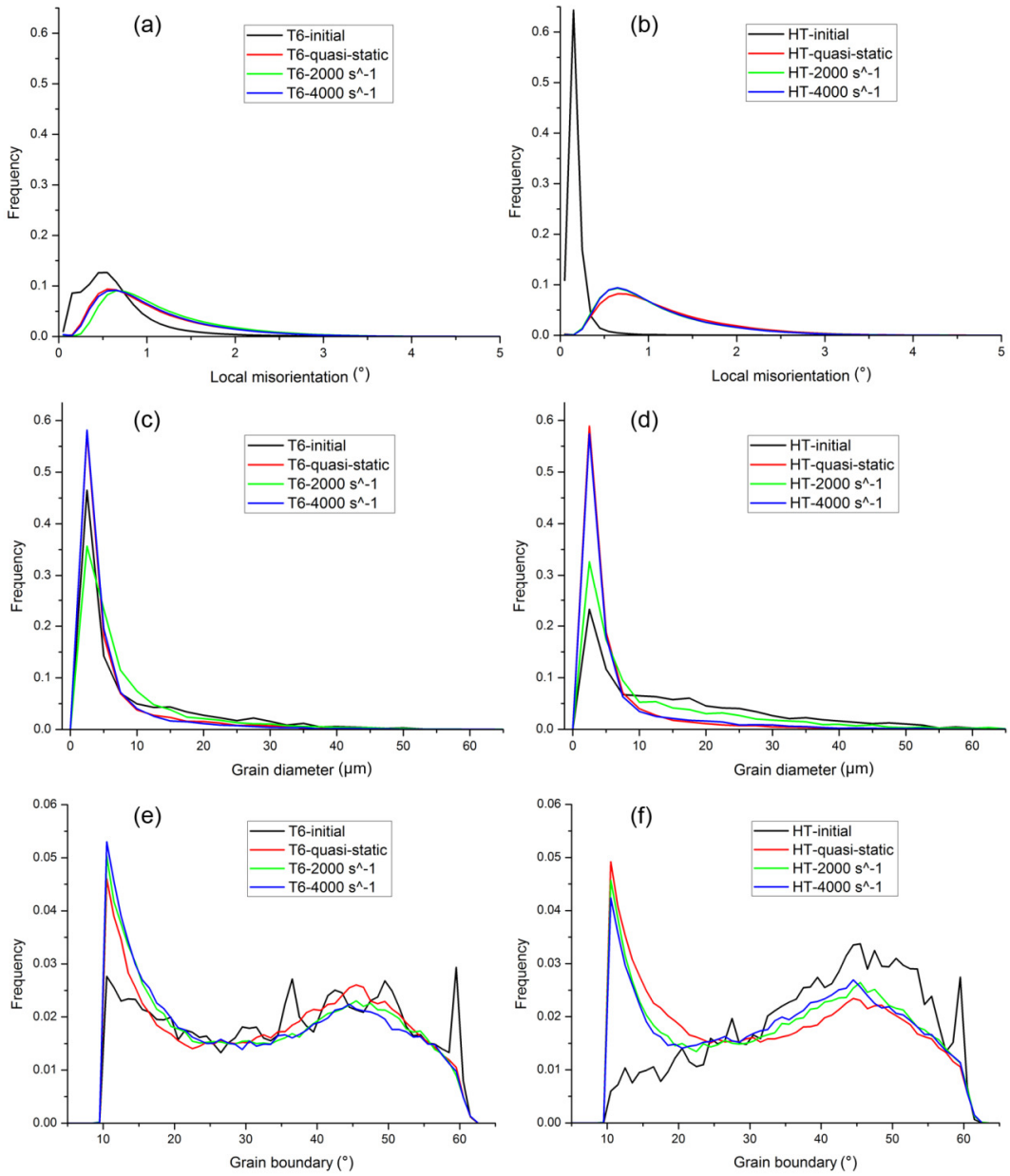

Fig. 5 Statistical distributions after compressions at different strain rates on T6 (left column) and HT (right column) specimens. (a) and (b) are local misorientation distributions, (c) and (d) are grain size distributions, and (e) and (f) are grain boundary distributions.

Texture evolution

The initial pole figures of T6 specimens along with those of the specimens deformed under different strain rates are given in Fig. 9. Similarly, the same comparisons for HT specimens are shown in Fig. 10. As can be seen from Fig. 9, the T6 specimens have a strong initial texture before compression (Fig. 9(a)), which has been changed to another texture during quasi-static compression (Fig. 9(b)). Nonetheless, it is interesting to see that the texture change is less significant in dynamic compression at strain rate of 2000 s^{-1} (Fig. 9(c)), and the texture of the specimen deformed at strain rate of 4000 s^{-1} (Fig. 9(d)) is close to its initial texture. In other words, the lower the strain rate applied, the more significant change in the texture will happen. A similar result can also be observed from the HT case, as shown in Fig. 10.

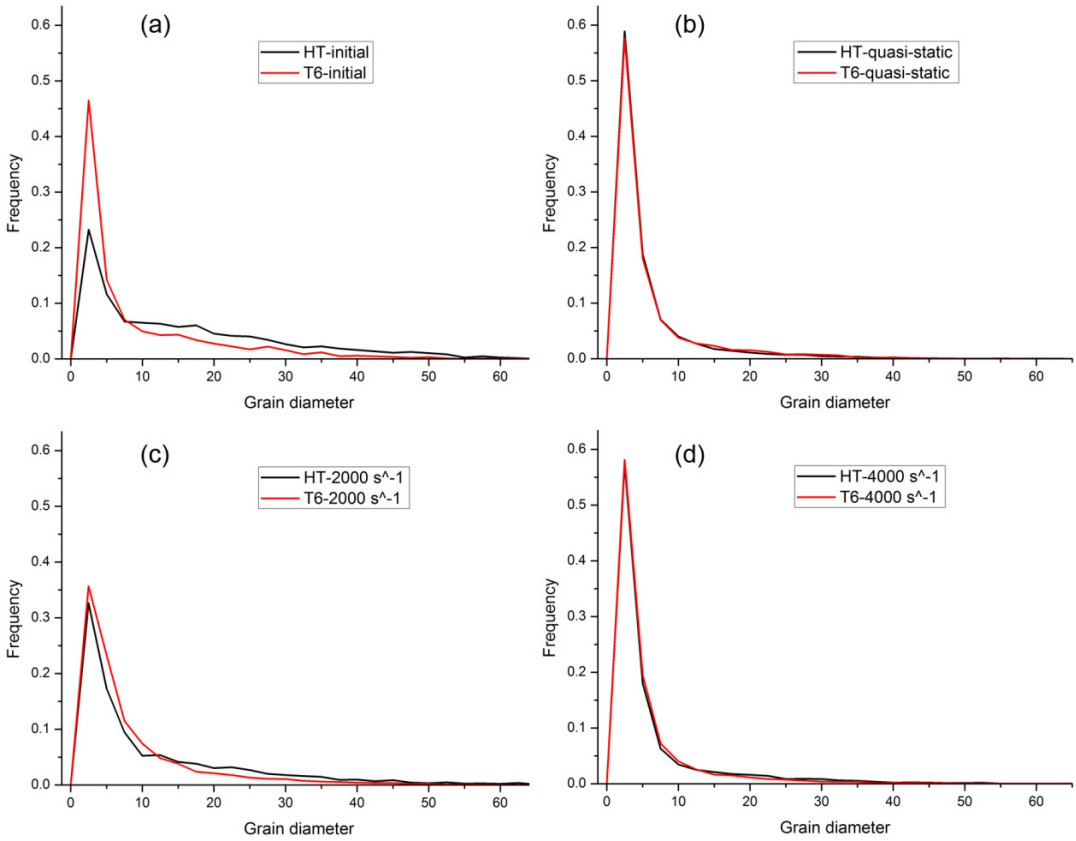

Fig. 6 Grain size distributions of T6 and HT specimens under (a) initial conditions and after compressions at strain rate of (b) 5×10^{-4} s^{-1}, (c) 2000 s^{-1} and (d) 4000 s^{-1}. (Unit: μm)

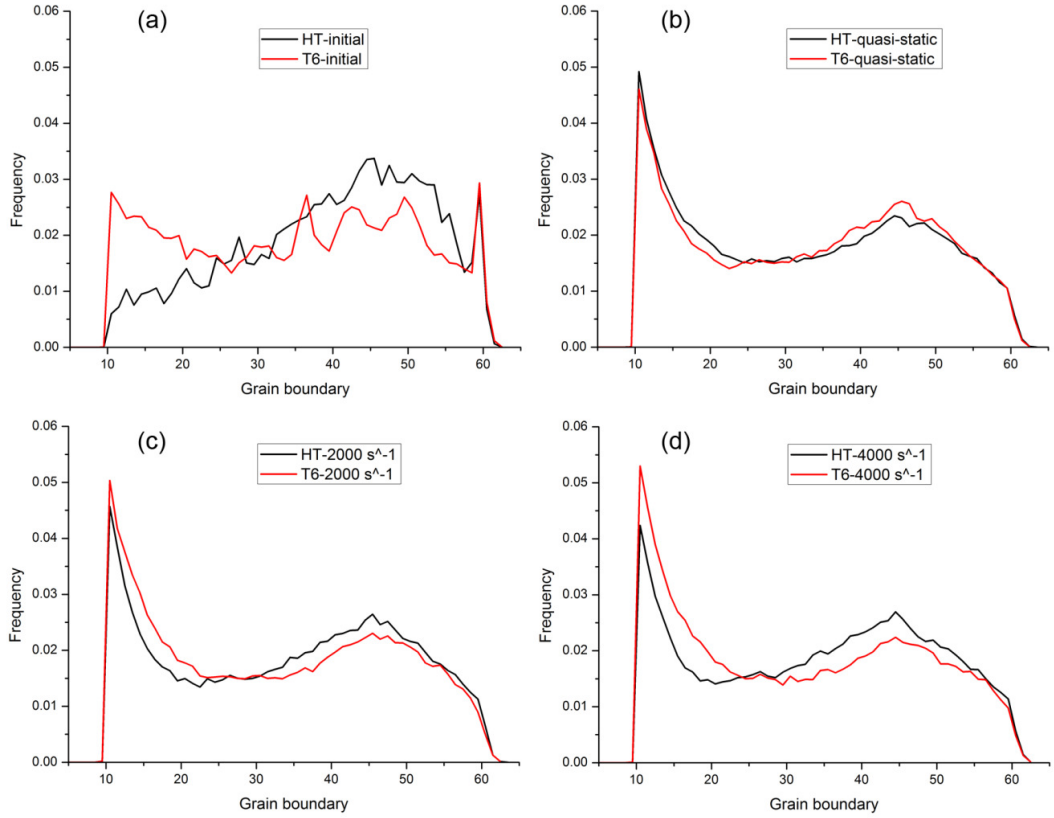

Fig. 7 Grain boundary distributions of T6 and HT specimens under (a) initial conditions and after compressions at strain rate of (b) 5×10^{-4} s^{-1}, (c) 2000 s^{-1} and (d) 4000 s^{-1}. (Unit: °)

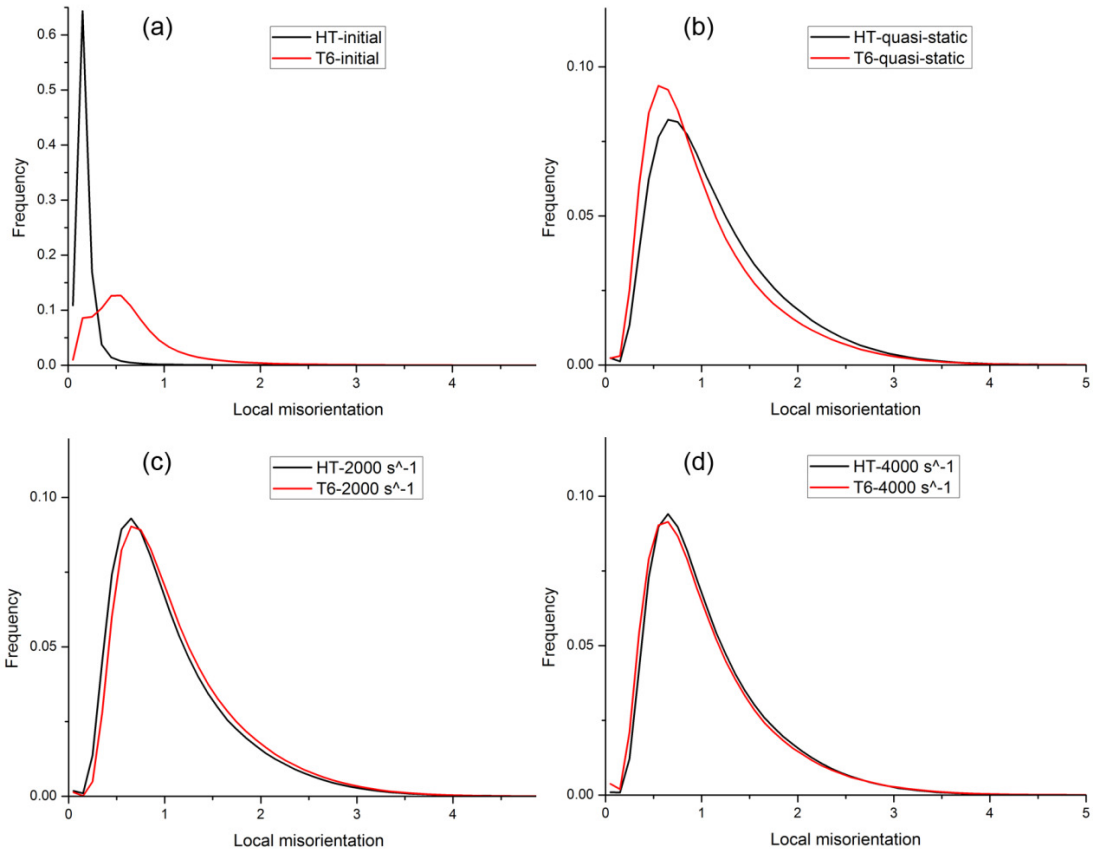

Fig. 8 Local misorientation distributions of T6 and HT specimens under (a) initial conditions and after compressions at strain rate of (b) 5×10^{-4} s^{-1}, (c) 2000 s^{-1} and (d) 4000 s^{-1}. (Unit: °)

Discussion

Effect of strain rate

As can be seen from Fig. 2, the yield strengths obtained from dynamic loading at strain rate of 4000 s^{-1} will be 17% and 19% higher than the quasi-static compression for T6 and HT specimens, respectively. Obviously, the strain rate has a strong effect on the strength of both T6 and HT specimens, where a larger increase of strength can be found in T6 specimens. This can be attributed to the denser pre-existing misorientations distributed in T6 specimens as shown in Fig. 3(a). The higher initial dislocation density in T6 specimens hinders the moving of newly created dislocations and therefore increases the strength of the material. In contrast, the effects of strain rate on grain size, grain boundary and local misorientation distributions are small, as shown in Fig. 5. Nonetheless, it can be seen from Fig. 5(c)-(f) that the strain rate effect on grain size and grain boundary distributions is slightly more significant in HT specimens than in T6 specimens.

The strain rate effect is also notable on the change of crystallographic texture. Both Figs. 9 and 10 show that the higher the strain rate applied, the less significant the change will be on the texture. It is observed in both T6 and HT specimens that, the texture after compression at the strain rate of 4000 s^{-1} is the closest to the initial texture while the texture after quasi-static compression has totally transformed. This can be explained by assuming that the dislocation motion is limited by surrounding dislocations and precipitates within such short deformation time period under high strain rates. Furthermore, the dislocations created in a very short time will be entangled in a local region rather than traveling to far away regions. Therefore, they will prevent the development of large slip deformations and significant texture change.

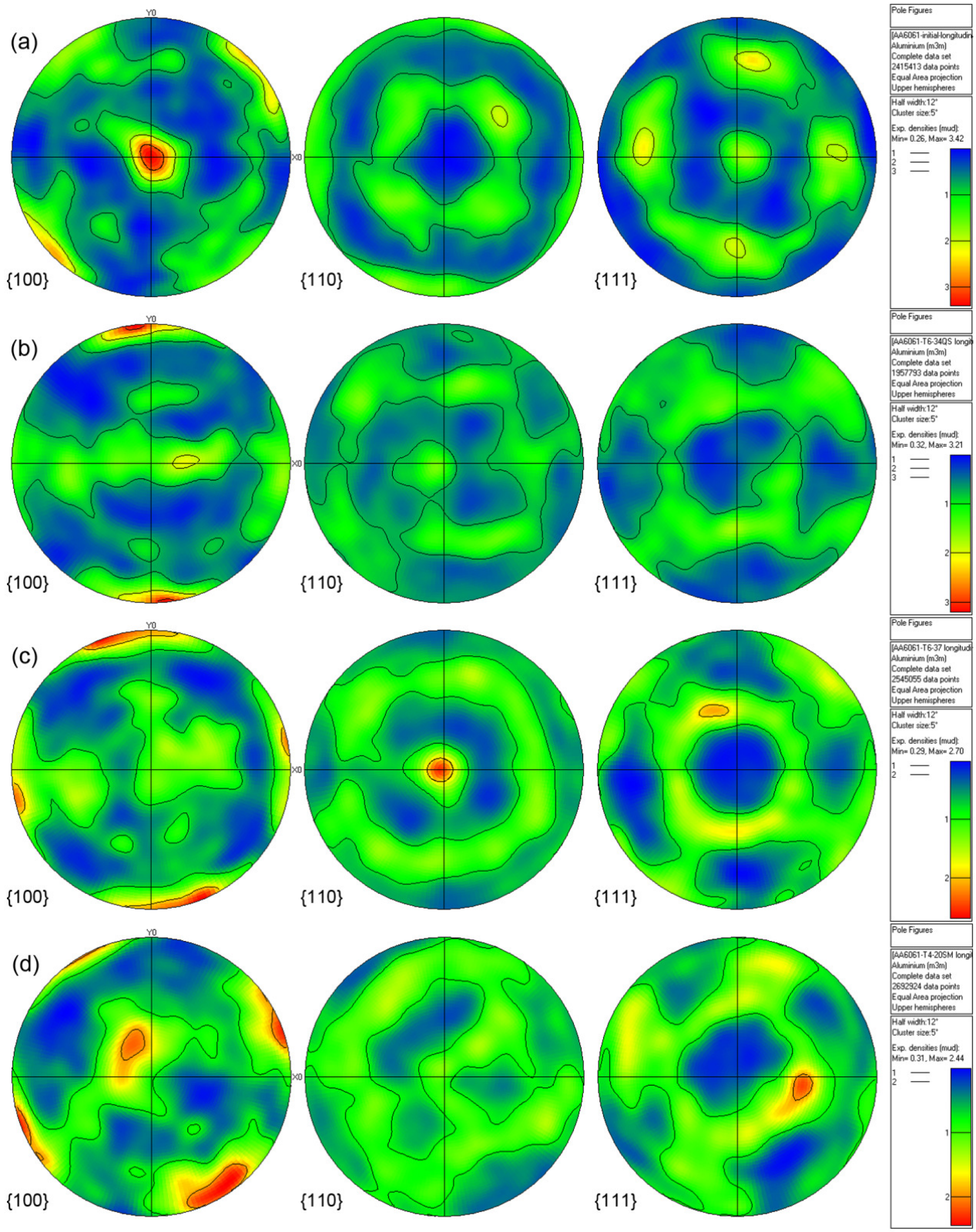

Fig. 9 Pole figures of T6 specimens with (a) initial conditions and after compressions at strain rate of (b) 5×10^{-4} s^{-1}, (c) 2000 s^{-1} and (d) 4000 s^{-1}.

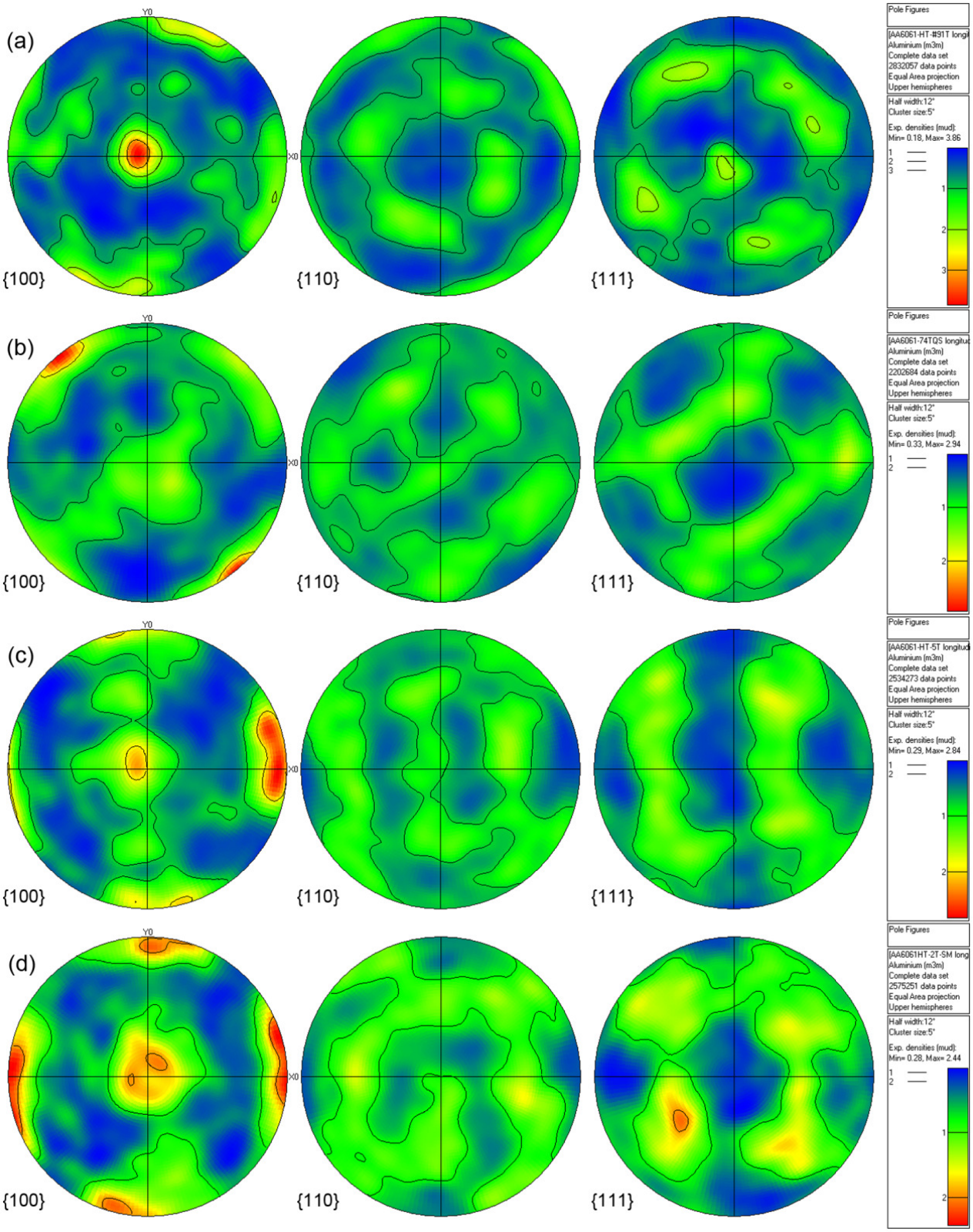

Fig. 10 Pole figures of T6 specimens with (a) initial conditions and after compressions at strain rate of (b) 5×10^{-4} s^{-1}, (c) 2000 s^{-1} and (d) 4000 s^{-1}.

Effect of heat treatment

Fig. 2 shows an obvious decrease in yield strength induced by the solution heat treatment and aging. The main reason for this result is that the solution heat treatment and aging process has reduced the initial dislocations density in the specimen and changed the shape and size of the precipitates (Poole et al. 2000; Senkov et al. 2008; Marlaud et al. 2010; Maisonnette et al. 2011). Therefore, it will be easier for compression induced new dislocations to appear and spread out in the specimen, rather than being entangled with existing dislocations as occurs in the T6 specimens. Since the dislocations created by compression can travel through the grains more freely, without disrupted by existing dislocations, the hardening behaviour of the HT specimens is supposed to be weaker than the T6 specimens. However, the grain size distribution after compression for both cases are almost the same, despite the fact that the initial grain size distributions are different, as shown in Fig. 6. Also it can be seen from Fig. 7 that, both T6 and HT specimens retain many high angle grain boundaries, which may obstruct dislocation motion through these grain boundaries. The concentration of dislocations at grain boundaries will most likely lead to initiation of micro-cracks, which is confirmed by the observations of micro-cracks initiation at the grain boundaries presented in the next section. Overall, the additional heat treatment and aging has remarkably decreased the yield strength regardless of strain rates, and has a small effect on grain size and local misorientation distributions.

Damage

Regardless of the strain rate applied, it is observed under SEM that micro-cracks appear in both T6 and HT specimens after compression. However, the number and typical size of micro-cracks are slightly different between the quasi-static and 4000 s^{-1} strain rate compressions. The SEM images of initial and compressed T6 specimens are given in Fig. 11. It is shown in Fig. 11(b)-(d) that the cracks tend to appear along grain boundaries under compressions at all strain rates. The typical crack length induced by quasi-static compression is larger than 4 μm (Fig. 11(b)), whereas the one caused by 4000 s^{-1} dynamic compression is usually less than 2 μm (Fig. 11(d)). Also the number of cracks after quasi-static compression is much higher than after the 4000 s^{-1} dynamic compression. The typical number and length of cracks after 2000 s^{-1} dynamic compression (Fig. 11(c)) are smaller than that after quasi-static compression but larger than that after 4000 s^{-1} dynamic compression. In fact, it is much easier to observe micro-cracks under SEM in quasi-static compressed specimens than in dynamic compressed specimens. Similar results are seen for the HT and T6 specimens. Although this cannot be clearly seen in Fig. 11(c) and 11(d) due to the small size of the area shown on the micrographs (several micrographs were taken for analysis but only one is shown for each specimen in this paper), much fewer micro-cracks can be found in the specimens after dynamic compression, and the crack size are also smaller. However, only qualitative observations can be made at this point.

It is believed that the abovementioned micro-crack observations are the results of the high strain rate effect. Since the compression is applied at a very high rate, it will lead to a consequence that the dislocations in the grains are not fully developed due to the very short deformation time. There are more small dislocations entangled with each other, preventing them forming a micro-crack. This is consistent with the observation that the texture has not been severely changed at high strain rate, as compared with the quasi-static case. Furthermore, similar typical crack length and density are observed for T6 and HT specimens deformed at the same strain rate, indicating that the effect of solution heat treatment and aging is not significant in terms of crack formation. The strain rate is observed to be the dominant factor in forming micro-cracks.

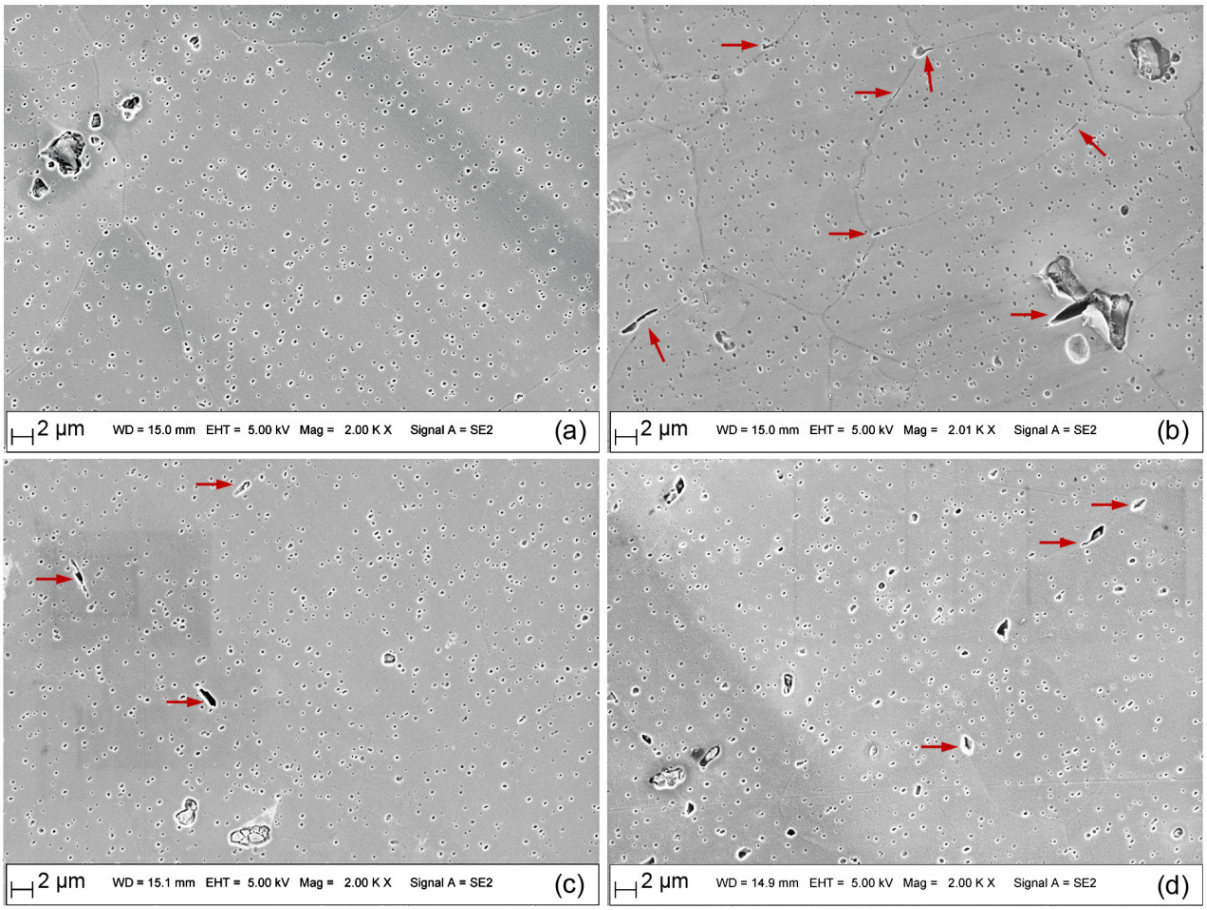

Fig. 11 Micro-cracks appeared on T6 specimens that are (a) as received and after compressions at strain rate of (b) 5×10^{-4} s^{-1}, (c) 2000 s^{-1} and (d) 4000 s^{-1}.

Conclusions

Dynamic compression experiments are conducted on as-received and solution heat treated specimens using the split Hopkinson bar to study the effects of strain rate and heat treatment on AA6061. Texture characterisation and initiation of micro-cracks after compression at different strain rates are obtained from EBSD scans and SEM micrographs to investigate the evolutions of microstructure and texture. As a result, the dynamic compression at strain rates of 4000 s^{-1} has increased the yield strengths of as-received and solution heat treated specimens by 17% and 19%, respectively. The solution heat treatment, however, dramatically reduced the yield strengths of quasi-static and 4000 s^{-1} dynamic compressions by 49.8% and 49.1%, respectively. Although the initial distributions of local misorientations, grain size and grain boundary angles are different in the as-received and solution heat treated specimens, the EBSD results show that these distributions are very similar for both types of specimens after compression. It is shown that the strain rate has a small effect on microstructural evolution. Nonetheless, it is observed that the higher the applied strain rate is, the less significant the change will be on the texture. Fewer micro-cracks and smaller crack size can be found in the dynamic compressed specimens than in the specimens that underwent quasi-static compression for both the HT and T6 specimens. Therefore, the strain rate is considered to be the dominant factor in forming micro-cracks.

Acknowledgements

The work was supported in part by the Australian Research Council through Centre of Excellence for Design in Light Metals (CE0561574), Discovery Projects (DP130101291 and DP140100945) and LIEF Project (LE100100045), and by the National Natural Science Foundation of China through Grant No. 11232003. The authors acknowledge the facilities, and the scientific and technical assistance, of the Australian Microscopy & Microanalysis Research Facility at the Australian Centre for Microscopy & Microanalysis at the University of Sydney.

References

Adrien, J., Maire, E., Estevez, R., Ehrstrom, J.C. and Warner, T. (2004) "Influence of the thermomechanical treatment on the microplastic behaviour of a wrought Al-Zn-Mg-Cu alloy", *Acta Materialia*, Vol. 52, pp. 1653-1661.

Flores-Johnson, E.A., Muránsky, O., Hamelin, C.J., Bendeich, P.J. and Edwards, L. (2012) "Numerical analysis of the effect of weld-induced residual stress and plastic damage on the ballistic performance of welded steel plate", *Computational Materials Science*, Vol. 58, pp. 131-139.

Garrett, R.P., Lin, J. and Dean, T.A. (2005) "An investigation of the effects of solution heat treatment on mechanical properties for AA 6xxx alloys: experimentation and modelling", *International Journal Of Plasticity*, Vol. 21, pp. 1640-1657.

Han, B.Q., Huang, J.Y., Zhu, Y.T. and Lavernia, E.J. (2006) "Strain rate dependence of properties of cryomilled bimodal 5083 Al alloys", *Acta Materialia*, Vol. 54, pp. 3015-3024.

Han, N.M., Zhang, X.M., Liu, S.D., He, D.G. and Zhang, R. (2011) "Effect of solution treatment on the strength and fracture toughness of aluminum alloy 7050", *Journal Of Alloys and Compounds*, Vol. 509, pp. 4138-4145.

Harnish, S.F., Padilla, H.A., Gore, B.E., Dantzig, J.A., Beaudoin, A.J., Robertson, I.M. and Weiland, H. (2005) "High-temperature mechanical behavior and hot rolling of AA705X", *Metallurgical and Materials Transactions a-Physical Metallurgy and Materials Science*, Vol. 36A, pp. 357-369.

Hoge, K. (1966) "Influence of strain rate on mechanical properties of 6061-T6 aluminum under uniaxial and biaxial states of stress", *Experimental Mechanics*, Vol. 6, pp. 204-211.

Johnsen, J., Holmen, J.K., Myhr, O.R., Hopperstad, O.S. and Børvik, T. (2013) "A nano-scale material model applied in finite element analysis of aluminium plates under impact loading", *Computational Materials Science*, Vol. 79, pp. 724-735.

Lassance, D., Fabregue, D., Delannay, F. and Pardoen, T. (2007) "Micromechanics of room and high temperature fracture in 6xxx Al alloys", *Progress In Materials Science*, Vol. 52, pp. 62-129.

Lee, W.S., Sue, W.C., Lin, C.F. and Wu, C.J. (2000) "The strain rate and temperature dependence of the dynamic impact properties of 7075 aluminum alloy", *Journal Of Materials Processing Technology*, Vol. 100, pp. 116-122.

Liu, X.Y., Pan, Q.L., Lu, Z.L., Cao, S.F., He, Y.B. and Li, W.B. (2010) "Effects of solution treatment on the microstructure and mechanical properties of Al-Cu-Mg-Ag alloy", *Materials & Design*, Vol. 31, pp. 4392-4397.

Ma, Z., Samuel, E., Mohamed, A.M.A., Samuel, A.M., Samuel, F.H. and Doty, H.W. (2010) "Influence of aging treatments and alloying additives on the hardness of Al-11Si-2.5Cu-Mg alloys", *Materials & Design*, Vol. 31, pp. 3791-3803.

Maisonnette, D., Suery, M., Nelias, D., Chaudet, P. and Epicier, T. (2011) "Effects of heat

treatments on the microstructure and mechanical properties of a 6061 aluminium alloy", *Materials Science and Engineering a-Structural Materials Properties Microstructure and Processing*, Vol. 528, pp. 2718-2724.

Marlaud, T., Deschamps, A., Bley, F., Lefebvre, W. and Baroux, B. (2010) "Influence of alloy composition and heat treatment on precipitate composition in Al-Zn-Mg-Cu alloys", *Acta Materialia*, Vol. 58, pp. 248-260.

Moustafa, M.A., Samuel, F.H. and Doty, H.W. (2003) "Effect of solution heat treatment and additives on the microstructure of Al-Si (A413.1) automotive alloys", *Journal Of Materials Science*, Vol. 38, pp. 4507-4522.

Mrowka-Nowotnik, G. and Sieniawski, J. (2005) "Influence of heat treatment on the microstructure and mechanical properties of 6005 and 6082 aluminium alloys", *Journal Of Materials Processing Technology*, Vol. 162, pp. 367-372.

Odeshi, A.G., Owolabi, G.M., Singh, M.N.K. and Bassim, M.N. (2007) "Deformation and fracture behavior of alumina particle-reinforced Al 6061-T6 composite during dynamic mechanical loading", *Metallurgical and Materials Transactions a-Physical Metallurgy and Materials Science*, Vol. 38A, pp. 2674-2680.

Oosterkamp, L.D., Ivankovic, A. and Venizelos, G. (2000) "High strain rate properties of selected aluminium alloys", *Materials Science and Engineering a-Structural Materials Properties Microstructure and Processing*, Vol. 278, pp. 225-235.

Ozturk, F., Sisman, A., Toros, S., Kilic, S. and Picu, R.C. (2010) "Influence of aging treatment on mechanical properties of 6061 aluminum alloy", *Materials & Design*, Vol. 31, pp. 972-975.

Poole, W.J., Saeter, J.A., Skjervold, S. and Waterloo, G. (2000) "A model for predicting the effect of deformation after solution treatment on the subsequent artificial aging behavior of AA7030 and AA7108 alloys", *Metallurgical and Materials Transactions a-Physical Metallurgy and Materials Science*, Vol. 31, pp. 2327-2338.

Sadeler, R., Totik, Y., Gavgali, M. and Kaymaz, I. (2004) "Improvements of fatigue behaviour in 2014 Al alloy by solution heat treating and age-hardening", *Materials & Design*, Vol. 25, pp. 439-445.

Senkov, O.N., Shagiev, M.R., Senkova, S.V. and Miracle, D.B. (2008) "Precipitation of Al-3(Sc,Zr) particles in an Al-Zn-Mg-Cu-Sc-Zr alloy during conventional solution heat treatment and its effect on tensile properties", *Acta Materialia*, Vol. 56, pp. 3723-3738.

Smerd, R., Winkler, S., Salisbury, C., Worswick, M., Lloyd, D. and Finn, M. (2005) "High strain rate tensile testing of automotive aluminum alloy sheet", *International Journal Of Impact Engineering*, Vol. 32, pp. 541-560.

Tucker, M.T., Horstemeyer, M.F., Whittington, W.R., Solanki, K.N. and Gullett, P.M. (2010) "The effect of varying strain rates and stress states on the plasticity, damage, and fracture of aluminum alloys", *Mechanics of Materials*, Vol. 42, pp. 895-907.

Wagenhofer, M., Erickson-Natishan, M., Armstrong, R.W. and Zerilli, F.J. (1999) "Influences of strain rate and grain size on yield and serrated flow in commercial Al-Mg alloy 5086", *Scripta Materialia*, Vol. 41, pp. 1177-1184.

Xu, Y.B., Zhong, W.L., Chen, Y.J., Shen, L.T., Liu, Q., Bai, Y.L. and Meyers, M.A. (2001) "Shear localization and recrystallization in dynamic deformation of 8090 Al-Li alloy", *Materials Science and Engineering a-Structural Materials Properties Microstructure and Processing*, Vol. 299, pp. 287-295.